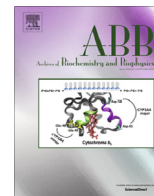




Contents lists available at ScienceDirect

Archives of Biochemistry and Biophysics

journal homepage: www.elsevier.com/locate/yabbi

A pre-steady state and steady state kinetic analysis of the N-ribosyl hydrolase activity of hCD157



Frank Preugschat^{a,*}, Luke H. Carter^b, Eric E. Boros^a, David J.T. Porter^{d,1}, Eugene L. Stewart^c, Lisa M. Shewchuk^c

^a Muscle Metabolism Discovery Performance Unit, GlaxoSmithKline, 5 Moore Drive, 3.2094, Research Triangle Park, NC 27709, United States

^b Platform Technology and Science, Molecular Discovery Research, Biological Sciences, GlaxoSmithKline, 5 Moore Drive, 3.2094, Research Triangle Park, NC 27709, United States

^c Platform Technology and Science, Molecular Discovery Research, Chemical Sciences, GlaxoSmithKline, 5 Moore Drive, 3.2094, Research Triangle Park, NC 27709, United States

^d GlaxoSmithKline, 5 Moore Drive, 3.2094, Research Triangle Park, NC 27709, United States

ARTICLE INFO

Article history:

Received 27 February 2014

and in revised form 10 September 2014

Available online 20 September 2014

Keywords:

Nicotinamide riboside

NAD⁺ salvage

CD38

CD157

ABSTRACT

hCD157 catalyzes the hydrolysis of nicotinamide riboside (NR) and nicotinic acid riboside (NAR). The release of nicotinamide or nicotinic acid from NR or NAR was confirmed by spectrophotometric, HPLC and NMR analyses. hCD157 is inactivated by a mechanism-based inhibitor, 2'-deoxy-2'-fluoro-nicotinamide arabinoside (fNR). Modification of the enzyme during the catalytic cycle by NR, NAR, or fNR increased the intrinsic protein fluorescence by approximately 50%. Pre-steady state and steady state data were used to derive a minimal kinetic scheme for the hydrolysis of NR. After initial complex formation a reversible step (360 and 30 s⁻¹) is followed by a slow irreversible step (0.1 s⁻¹) that defined the rate limiting step, or *k_{cat}*. The calculated *K_{Mapp}* value for NR in the hydrolytic reaction is 6 nM. The values of the kinetic constants suggest that one biological function of cell-surface hCD157 is to bind and slowly hydrolyze NR, possibly converting it to a ligand-activated receptor. Differences in substrate preference between hCD157 and hCD38 were rationalized through a comparison of the crystal structures of the two proteins. This comparison identified several residues in hCD157 (F108 and F173) that can potentially hinder the binding of dinucleotide substrates (NAD⁺).

© 2014 Elsevier Inc. All rights reserved.

Introduction

Nicotinamide adenine dinucleotide (NAD⁺)² is a cofactor in over 400 oxidation–reduction reactions. NAD⁺ is also used in protein poly/mono ADP-ribosylation, protein deacetylation, transcriptional repression, vitamin biosynthesis and gene splicing reactions [1–5].

* Corresponding author. Fax: +1 (919) 315 6964.

E-mail address: Frank.X.Preugschat@gsk.com (F. Preugschat).

¹ Retired.

² Abbreviations used: hCD38, CD38, human CD38; CD157, BST-1, human CD157; ADP, adenosine diphosphate; ARC, *Aplysia* ADP-ribosyl cyclase; fNR, 2'-deoxy-2'-fluoro-nicotinamide arabinoside; NAD⁺, nicotinamide adenine dinucleotide; cADPR, cyclic adenosine diphosphate ribose; NADP⁺, nicotinamide adenine dinucleotide phosphate; BST-1, bone marrow stromal antigen 1; NR⁺, NR, nicotinamide riboside; NMN, NMN⁺, nicotinamide mononucleotide; NAR, nicotinic acid riboside; Nam, nicotinamide; R, ribose; R-5-P, ribose-5-phosphate; GPI, glycosylphosphatidylinositol; [NR], the concentration of NR in a given experiment; [NAR], the concentration of NAR in a given experiment; [fNR], the concentration of fNR in a given experiment; E, enzyme; E * R, covalent complex between E and Ribose; LC/MS, liquid chromatography mass spectrometry; GSK, GlaxoSmithKline.

Pharmacological stimulation of NAD⁺ synthesis or inhibition of NAD⁺ degradation has therapeutic promise for the treatment of a number of human conditions and diseases in which NAD⁺ levels are decreased relative to the normal state [6–11]. For example, perturbed NAD⁺ metabolism occurs in pellagra, which is easily cured by niacin supplementation [12]. Successful pharmacological intervention in the disease state is dependent upon a fundamental understanding of the anabolic and catabolic enzymes involved in producing the NAD⁺ deficit.

Aplysia ADP-ribosyl cyclase (ARC) is the first member of a family of NAD⁺ metabolizing enzymes (E.C.3.2.2.5) to be characterized [13]. The enzyme catalyzes the formation of nicotinamide (Nam) and the calcium mobilization hormone cyclic adenosine diphosphate ribose (cADPR) from NAD⁺, with retention of the β-stereochemistry at the C1'-ribose residue. The mammalian paralog, CD38, is primarily a hydrolytic enzyme of the pyridine nucleotides, NAD⁺, NADP⁺ and NMN. Using NAD⁺ as substrate CD38 catalyzes the formation of approximately 1% cADPR and 99% ADPR and Nam. These enzymes also efficiently catalyze selected base-exchange reactions with Nam analogs (and pyridine

nucleotides) that has been used to characterize and isolate alternative substrates and inhibitors of these enzymes [14–17].

CD157 (often referred to as; bone marrow stromal antigen BST-1, NAD⁺ nucleosidase or cyclic ADP-ribose hydrolase 2) was initially cloned by differential screening of synovial fluid from patients with a severe form of rheumatoid arthritis [18–19]. The gene for this enzyme is located on human chromosome 4 (4p15.33) and is a product of gene duplication of the CD38 locus [20]. The exon structure and gene regulatory elements are highly conserved between CD38 and CD157. Because hCD157 is a younger gene than hCD38, the human protein is 78–89% identical to the mouse and rat homolog, respectively. Despite their common ancestry there are notable differences. CD38 is an integral membrane protein, whereas CD157 is associated with the cellular membrane through a C-terminal glycosylphosphatidylinositol (GPI) linkage [20]. CD38 is a powerful hydrolytic catalyst (NAD⁺ k_{cat}/K_M value of $10 \mu\text{M}^{-1} \text{s}^{-1}$), whereas CD157 is an ineffective (NAD⁺ and NGD⁺ k_{cat}/K_M value of $0.2\text{--}1 \text{mM}^{-1} \text{s}^{-1}$) hydrolytic catalyst [15,21–22]. In summary CD157 is a protein with novel, but related biochemical properties.

Nicotinamide riboside (NR) was initially characterized in the 1940s and was recently shown to function as a precursor vitamin for eukaryotic NAD⁺ biosynthesis [23–24]. Intracellular phosphorylation of NR produces NMN, an intermediate that is then subsequently adenylated to form NAD⁺ in the NAD⁺ salvage pathway. Because exogenously-added NR raises intracellular NAD⁺ levels in mammalian cells (2–3-fold) NR could be a dietary supplement that elevates NAD levels [25]. It is possible that inhibition of NR catabolism may be a potential mechanism for increasing cellular NAD⁺ levels.

During the course of characterizing the biochemical selectivity of CD38 inhibitors, we discovered that hCD157 prefers NR over NAD⁺ as a substrate for hydrolysis (k_{cat}/K_M value of $17 \mu\text{M}^{-1} \text{s}^{-1}$). Herein, we present evidence that the enzyme uses covalent catalysis with formation of a ribosylated enzyme intermediate. In the absence of nicotinamide, the level of ribosylated enzyme is high at low levels of NR. Thus the enzyme is effectively capturing the ribose portion of NR at very low levels of NR. The proposed ribosylated intermediate is relatively long-lived, suggesting that NR may function to activate hCD157 as a receptor. Alternative substrates (analogs of NR) or antagonists (inhibitors) of hydrolytic function may prove to be useful therapeutic agents for the treatment of a number of human diseases.

Materials and methods

Materials

NAD⁺, NMN, nicotinamide, alkaline phosphatase, phosphate buffered saline (PBS), Hepes, nicotinic acid, and EDTA were from Sigma Chemical Co. hCD157 (catalog number 4736-AC, lot # RLZ0311071) was purchased from R & D Systems, Minneapolis, MN or from Repronkine Ltd., Rehovot, Israel (catalog number RKQ 10588). NR was purchased from Toronto Research Chemicals.

Purification of recombinant proteins

Our initial characterization of two commercially available hCD157 proteins revealed biochemical differences between the proteins. Due to these differences we decided to clone, express and purify hCD157. hCD157 amino acids 29–303 with a N-terminal histidine tag and a TEV cleavage site were cloned into a Bacmam expression vector for Bacmam virus production [26]. Bacmam virus was used to transfect CHO cells and cell culture supernatants were harvested 72 h post-infection. 10 L of conditioned cell culture

media was concentrated using 10 kDa cutoff Pall filters. The concentrate was buffer-exchanged with 20 L of 25 mM Hepes pH 7.5, 250 mM NaCl, and was re-concentrated to 2 L final volume. This concentrate was initially purified on a nickel Sepharose column and eluted using imidazole. The N-terminal histidine tag was removed by digestion with TEV protease and the enzyme was then reapplied to a nickel Sepharose column. The flow-through fraction was collected and applied to a superdex 75 sizing column, equilibrated with buffer. Peak fractions were concentrated and stored frozen. Peptide sequencing of trypsin-digested hCD157 fragments confirmed the identity of the purified protein.

CD38 (E226Q) protein purification

10 L of conditioned media from *Pichia pastoris* – expressing human CD38 (N100D, N164A, N209D, N219D, E226Q with a N-terminal histidine tag and TEV protease cleavage site) was applied to a nickel Sepharose column. The column was washed with buffer, (25 mM Hepes pH 7.5, 250 mM NaCl, 50 mM imidazole) and protein was eluted with buffer (25 mM Hepes pH 7.5, 250 mM NaCl, 250 mM imidazole). The histidine tag was removed by digestion with TEV protease and was chromatographed on a superdex 75 sizing column. Fractions containing CD38 were pooled and passed over a nickel Sepharose column to remove any CD38 containing the histidine tag. Flow-through fractions containing CD38 were pooled and concentrated to 5 mg/mL. Sequence identity with CD38 was confirmed by LC/MS amino acid sequence analysis of trypsin-digested peptides. The enzyme was >95% pure.

Crystallographic analyses of a binary complex of NMN with the hCD38 catalytic mutant E226Q

Human CD38 E226Q in 25 mM Hepes pH 7, 200 mM NaCl was concentrated to approximately 7 mg/mL. 5 mM NMN was added to the protein and the complex was incubated on ice for 1 h. Crystals were grown by hanging drop vapor diffusion in 24-well Linbro trays at room temperature in 23% PEG3350, 0.1 M BTP, pH 8.5. Crystals were harvested after 1 day and flash frozen in PFO prior to data collection. Data were collected in house on a Sat944⁺ detector and Rigaku FRE rotating anode generator. Data were processed using HKL2000 [27]. The structure was solved by molecular replacement using MOLREP [28] and 1YH3 (human CD38 extracellular domain) as a starting model [29]. The structure was rebuilt and refined using CCP4 [30] and Coot [31]. Coordinates have been deposited in the RCSB database as PDB code (4OGW).

Assay of hydrolytic activity

Hydrolysis of the nicotinamide ribose bond was monitored through a decrease in absorbance of the nucleos(t)ide [32]. The values of the difference extinction coefficients used were: $\Delta\epsilon_{262} = -1.4 \text{mM}^{-1} \text{cm}^{-1}$ for NR, $\Delta\epsilon_{280} = -1.2 \text{mM}^{-1} \text{cm}^{-1}$ for NMN and NAD⁺, $\Delta\epsilon_{280} = -1.7 \text{mM}^{-1} \text{cm}^{-1}$ for NAR.

HPLC analyses of hCD157-catalyzed NR hydrolysis

Standards and reaction products were analyzed on a Agilent 1100 series HPLC, using a 10 cm reverse phase C18 column (Phenomenex). 50 mM ammonium acetate, pH 7.0 was used for mobile phase A. 33 mM ammonium acetate, pH 7.0 in 70% acetonitrile was used for mobile phase B. A gradient of 0–100% mobile phase B was run over a 10 min time-course. Analytes were detected using a diode array spectrophotometer.

Reaction time-course analyses

The time-course for the reaction of substrate with hCD157 was monitored by the monophasic increase in intrinsic protein fluorescence associated with complex formation. On average 3–6 fluorescence tracings were averaged per analysis. After correcting the time-course for changes in protein fluorescence that occurred due to photo-bleaching, it was analyzed according to Eq. (1).

$$F(t) = F_1 * e^{-k_{obs} * t} + F_0 \quad (1)$$

where $F(t)$ was the observed signal at time equal to t , F_1 was the value of the amplitude, F_0 was the value of the final fluorescence, and k_{obs} was the value of the observed rate constant.

General methods

The Standard Buffer was PBS (Na^+), 1 mM EDTA at pH 7.1 and 25 °C. When high concentrations of bases/acids/reagents (nicotinic acid, nicotinamide, methanol) were used in the experiments, 50 mM Hepes pH 7.0, 1 mM EDTA was substituted for the Standard Buffer. Steady-state fluorescence spectra were recorded with a JASCO FP-6500 spectrofluorometer. Absorbance and conventional steady-state kinetic data were obtained from a UVIKON XL spectrophotometer. Pre-steady state kinetic reactions were monitored on an Applied Photophysics SX.20 Spectrophotometer (Leatherhead, UK). Entrance and exit slits were 2 mm in the fluorescence mode, and a >335 nm cutoff filter was used for protein fluorescence ($\lambda_{ex} = 290$ nm) measurements. All reported concentrations for stopped-flow experiments were final concentrations after mixing of reagents. The appropriate equations were fitted to the data by nonlinear least squares analyses using SigmaPlot from Jandel Scientific (Corte Madera, CA), or modeled using Dynafit software (Biokin Ltd., Watertown, MA). hCD157 was stored frozen at -20 °C. The enzyme was stable to several freeze thaw cycles and could be stored at 4 °C for greater than one month without loss of activity.

Results

Steady-state hydrolysis of NR

Time-dependent changes in the UV properties of NR in the Standard Buffer were observed upon addition of hCD157. Similar changes were observed in 50 mM Hepes pH 7.0, 1 mM EDTA. The reaction was not dependent on phosphate or on pyrophosphate. The UV difference spectrum of the spent solution with enzyme vs a solution lacking enzyme revealed a maximal absorbance change at 262 nm. The normalized difference spectrum was identical to that predicted from the hydrolysis of NR. Using an extinction coefficient of $5600 \text{ M}^{-1} \text{ cm}^{-1}$ at 262 nm [32], the change in the NR extinction coefficient was $1400 \text{ M}^{-1} \text{ cm}^{-1}$. With $S_0 = 15 \mu\text{M}$, the progress curve was linear until over 95% of the NR was consumed. This indicated a very low K_M value for NR, without noticeable product inhibition (black trace, Fig. 1A). No inhibition by ribose was observed (at 5 mM), but Nam was a modest inhibitor of the enzyme (see below). Equilibration of the enzyme with 100 μM fNR completely inhibited the hydrolytic reaction, with no recovery of activity over the time-course (blue trace, Fig. 1A). No reaction with NAD^+ in the hydrolytic reaction was observed over a similar time-course (Fig. 1B). HPLC and NMR analyses of the hCD157-catalyzed hydrolysis reaction with NR clearly show nicotinamide is a product of the reaction (Fig. 1C, Supplemental Figs. 5 and 7).

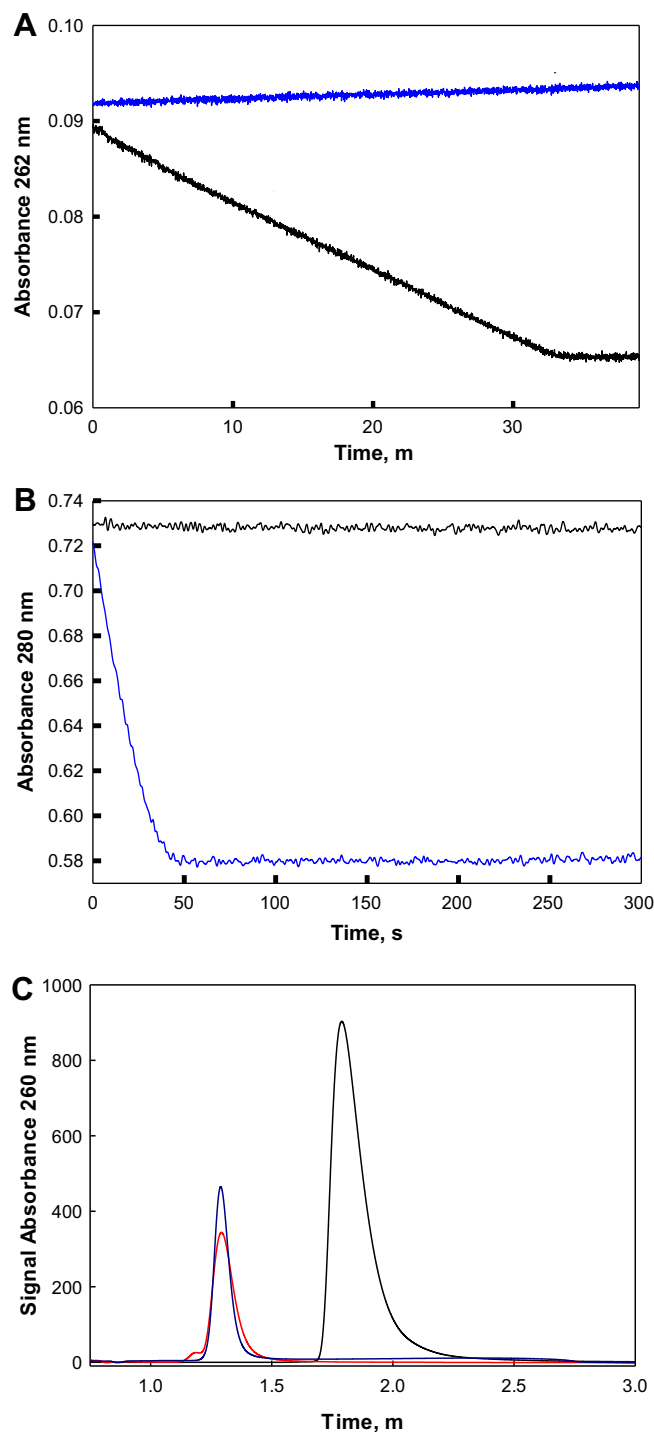


Fig. 1. (A) Steady-state progress curve analyses of the hCD157-catalyzed hydrolysis of NR. 80 nM hCD157 was added to 15 μM NR. Reaction progress was followed at 262 nm (black trace). Enzyme (8 μM) was pre-incubated for 10 min with 100 μM fNR, then diluted 100-fold into Standard Buffer containing 15 μM NR (blue trace). No activity was observed over the time-course. (B) Steady-state progress curve analyses of the hCD157-catalyzed hydrolysis of NAD^+ . The reaction was initiated by addition of 1 μM hCD157 to 160 μM NAD^+ in Standard Buffer and the hydrolysis of NAD^+ was followed at 280 nm (black trace). hCD38 (20 nM, blue trace) was used as a positive control for the hydrolysis of NAD^+ . (C) HPLC analyses of the hCD157-catalyzed NR hydrolysis reaction. 5 μL of NR (100 μM) was fractionated on a reversed phase C18 column and the absorbance at 260 nm was monitored by diode array. NR (black trace) eluted at 1.83 min. Nam eluted at 1.3 min (blue trace). hCD157-catalyzed hydrolysis of NR (red trace). NR was completely hydrolyzed to Nam. (For interpretation of the references to color in this figure legend, the reader is referred to the web version of this article.)

Table 1
 k_{cat} and K_M values for nucleos(t)ide hydrolysis.

Enzyme/substrate	K_M (μM)	k_{cat} (s^{-1})	k_{cat}/K_M ($\mu\text{M}^{-1} \text{s}^{-1}$)
hCD38/NMN ^a	150	500	3.3
hCD157/NR	0.006	0.1	17
hCD157/NAD ^b	NM	NM	0.0002
hCD157/NGD ^b	600	NM	0.001
hCD157/NAR	22	0.095	0.0045

^a [15].

^b [19,21,22].

A summary of the measured kinetic constants for NR and NAR is presented in Table 1. The k_{cat}/K_M value for the hCD157-catalyzed hydrolysis of NR is >10,000-fold higher than that for NAR, the next best natural substrate. This is primarily due to the remarkably low K_M value (6 nM calculated, see below). Because the steady-state K_M value for NR was low nanomolar it was not possible to experimentally determine the K_M value from absorbance-based steady state data. Pre-steady state methods were used to measure the K_M value (see below).

Pre-steady state analyses of the reaction of hCD157 with NR

Addition of NR to 200 nM hCD157 in the Standard Buffer increased the intrinsic protein fluorescence in a time- and concentration-dependent manner (Fig. 2A). Stopped-flow analysis of the early phase of the time-course revealed a rapid mono-phasic first order increase (k_{obs}) in fluorescence that was dependent on [NR]. The increase in k_{obs} values was hyperbolically dependent on [NR]. The data were consistent with a rapid, fluorescently-silent binding event ($E + NR$ in Scheme 1) followed by a conformational transition with a concomitant increase in protein fluorescence ($E(NR) \rightarrow E^*R$) in the absence of Nam, Scheme 1). The K_D value for [NR] was $22 \pm 1 \mu\text{M}$. The addition of Nam to the reaction increased the k_{obs} values (Scheme 2 and Fig. 2B). This is due to the contribution of k_{-2} to the overall reaction rate.

The value of the intercept and the value for K_N was estimated (Scheme 2) from data obtained in stopped-flow experiments. A single fixed NR concentration ($70 \mu\text{M}$, Fig. 2B) and various Nam concentrations were used to determine K_N and k_{-2} . In this experiment the maximal observed rate was greater ($k_2 + k_{-2}$, $380 \pm 10 \text{ s}^{-1}$) and the midpoint of the hyperbolic equation fit to the data represents the K_N for Nam in the $E^*R(\text{Nam})$ complex ($K_N = 320 \pm 60 \mu\text{M}$). The difference between the maximal observed rate constant and the intercept (k_{-2} , $31 \pm 2 \text{ s}^{-1}$) is rate of the reverse reaction to reform $E(\text{NR})$ (Scheme 1). The fluorescence of the ES complex was inferred to be approximately 90% that of free E by analysis of the amplitude changes observed, as free E was converted to E^*R and $E^*R(\text{Nam})$. Because the K_N for Nam was large ($320 \mu\text{M}$, Scheme 1 and Fig. 2B) and the addition of Nam to E^*R was a rapid equilibrium step, the formation of the E^*R intermediate was primarily responsible for the large increase in protein fluorescence (see below).

The K_M value for NR hydrolysis was estimated to be low nanomolar from visual inspection of progress curve data and calculated to be 6 nM from the measured pre-steady state kinetic constants (Scheme 3). The high affinity for NR made it possible to measure NR hydrolysis under single turnover conditions, where $[E] > [S]$. Binding of 375 nM NR to 750 nM hCD157 was biphasic. The initial rapid step of increasing fluorescence was followed by a slow first-order decay of enzyme fluorescence to baseline (free E). The k_{obs} value for the slow phase (Fig. 2C) was equated to the k_{cat} value (0.1 s^{-1}). Nam inhibited the single turnover kinetics (blue trace) by increasing the K_M for NR and decreasing the observed first

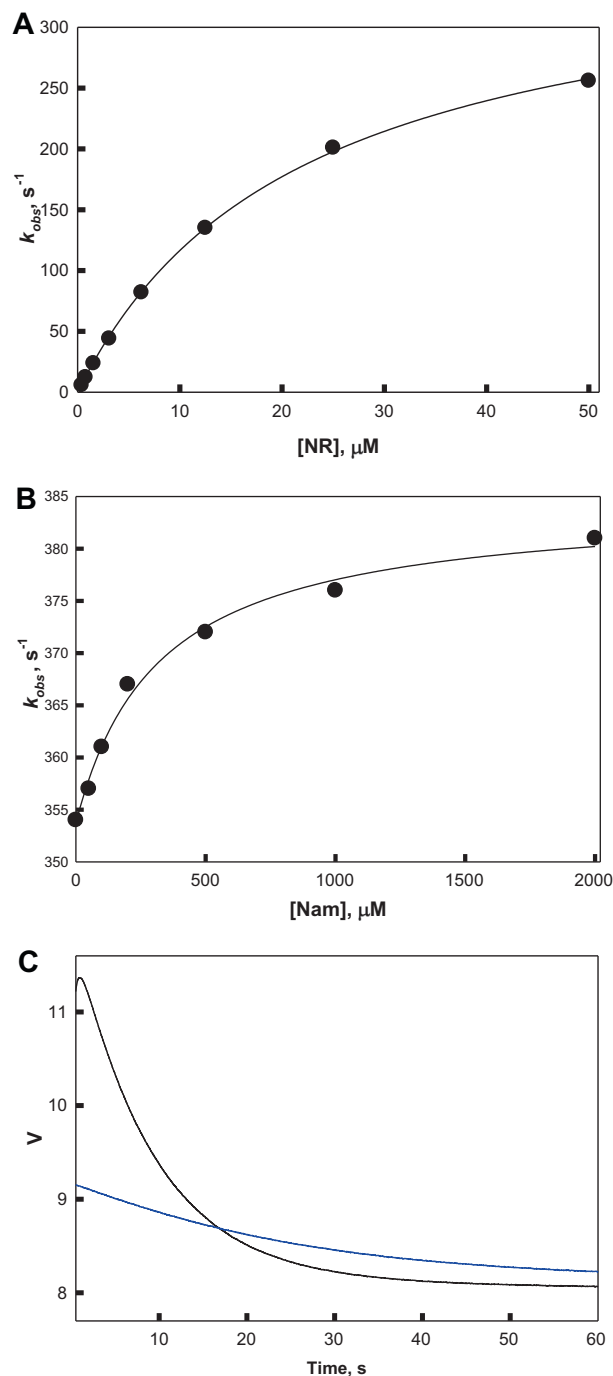
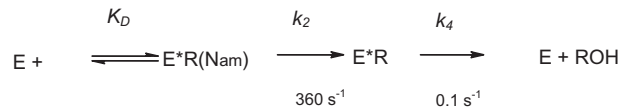
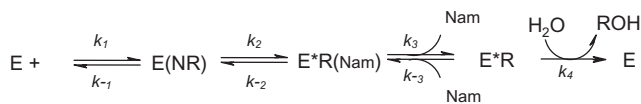


Fig. 2. (A) Pre-steady-state kinetics of the reaction of hCD157 with NR. A hyperbola was fitted to the first order rate constant values for the reaction with NR with 200 nM hCD157. The asymptote (370 s^{-1} , k_2) and midpoint ($22 \mu\text{M}$, K_D values) for initial complex formation were calculated from data collected in the absence of Nam. (B) Pre-steady-state kinetics of the reaction of hCD157 with NR in the presence of Nam. A hyperbola was fitted to the first order rate constant values for the reaction with NR. The asymptote (385 s^{-1} , $(k_2 + k_{-2})$) and the K_N ($330 \mu\text{M}$) for Nam were determined. The intercept (k_2 , at $[\text{Nam}] = 0$, 355 s^{-1}) was subtracted from the amplitude ($k_2 + k_{-2}$, 385 s^{-1}) to determine k_{-2} (30 s^{-1}), which is the rate constant for the formation of $E(\text{NR})$ from $E^*R(\text{Nam})$. (C) Single turnover kinetics of NR hydrolysis. 750 nM hCD157 in Standard Buffer was added to 375 nM NR. A double exponential was fitted to the biphasic change in protein fluorescence (black trace). The initial phase of increased protein fluorescence corresponded to the conversion of $E(\text{NR})$ to E^*R . The slow decrease in fluorescence ($k_{obs} = 0.1 \text{ s}^{-1}$) represents the decay of E^*R to free E, defining the rate-limiting step or k_{cat} . Addition of 250 μM Nam inhibited the reaction (blue trace). (For interpretation of the references to color in this figure legend, the reader is referred to the web version of this article.)



Scheme 1. A minimal kinetic scheme for the hydrolysis of NR, in the absence of Nam.

order rate constant (k_{obs}). Equations describing the effect of product inhibition on K_M and V_m are provided in the [Supplemental Methods](#).

Pre-steady state and steady state analyses of the reaction with NAR

Addition of NAR to 200 nM hCD157 in the Standard Buffer increased the intrinsic protein fluorescence in a time- and concentration-dependent manner (Fig. 3A). The increase in k_{obs} values was hyperbolically dependent on [NAR]. The limiting value was (k_2 , $2.3 \pm 0.1 \text{ s}^{-1}$). The K_D value for [NAR] was $300 \pm 40 \mu\text{M}$. Because the K_M value for NAR was in the micromolar range, initial rates of hydrolysis could be obtained using absorbance-based steady state methods. The initial rate data and the pre-steady state data both predicted the k_{cat}/K_M value for hydrolysis of NAR to be $4500 \text{ M}^{-1} \text{ s}^{-1}$. The K_{Mapp} value for hydrolysis of NAR was $22 \mu\text{M}$ vs 6 nM for NR. These results were consistent with NR and NAR forming the same catalytic intermediate, that was hydrolyzed (Fig. 3B) at the same rate (k_{cat} , 0.1 s^{-1}). NMR analyses of the hCD157-catalyzed hydrolysis reaction with NAR clearly show the release of NA from NAR (Supplemental Figs. 6 and 7).

Pre-steady state analyses of the reaction of hCD157 with fNR

Addition of fNR to 100 nM hCD157 in the Standard Buffer increased the intrinsic protein fluorescence in a time- and concentration-dependent manner (Supplemental Fig. 1A). The magnitude of the fluorescence increase was similar to that observed for NR but the kinetics of the reaction differed significantly (0.04 vs 360 s^{-1}). The time-course was a monophasic increase in fluorescence that was hyperbolically dependent on [fNR]. At saturating [fNR] the value of k_{obs} (k_2) was 0.04 s^{-1} and the K_D was $22 \pm 2 \mu\text{M}$ (Supplemental Fig. 1B). A summary of the measured kinetic constants is presented in Supplemental Table 1. Addition of Nam to a solution of E^*R quenched the fluorescence of the intermediate, allowing steady state measurement of a K_D for Nam (K_N). No recovery of enzyme activity was noted after several hours, thus the E^*R adduct was very stable. Trypsin-digested peptide fragments of

$$K_{mapp} = \frac{K_D}{1 + k_2/k_4} = 6 \text{ nM}$$

$$k_{cat} = \frac{k_2^*k_4}{k_2 + k_4} = 0.1 \text{ s}^{-1}$$

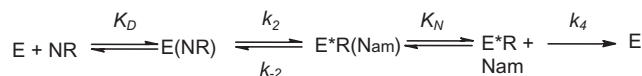
With [N] = 0 and $k_{-3} \ll (k_2 + k_4)$ Scheme (1) reduces to Scheme (3). Where $K_D = (k_{-1}/k_1)$.

Scheme 3. Derivation of k_{cat} and K_{Mapp} using measured K_D , k_2 and k_4 values.

fNR-modified hCD157 were sequenced using LC/MS methods and a single modified peptide was identified (Supplemental Fig. 1C). The 13-residue peptide contained a single glutamate residue (E178) that is structurally equivalent to the catalytic residue (E226) in CD38 that is modified by fNMN [14].

Discussion

CD157 or BST-1 (NAD⁺ nucleosidase, cyclic ADP-ribose hydrolase 2) arose approximately 500 million years ago through gene duplication of CD38 and today has only 36% sequence identity with CD38. Initial biochemical characterization determined that hCD157 is a weak NAD⁺ hydrolase and ADP-ribosyl cyclase (k_{cat}/K_M value for NAD of $200 \text{ M}^{-1} \text{ s}^{-1}$). Our experiments have shown that this enzyme has evolved to recognize, bind and hydrolyze NR with a k_{cat}/K_M value of $17 \mu\text{M}^{-1} \text{ s}^{-1}$. The exquisite selectivity/sensitivity of hCD157 for NR is primarily determined by a very low K_M value (6 nM). The minimal kinetic mechanism summarized in Scheme 1 describes the kinetic steps and constants used in the hCD157-catalyzed hydrolysis of NR. After initial complex formation (K_D , k_1 , k_{-1}), a reversible chemical step (k_2 , k_{-2}) is followed by an ordered release of products (as shown by k_3 , k_{-3} with Nam released first). The enzyme intermediate is hydrolyzed (k_4) to regenerate free enzyme and release ribose. The biochemical data was consistent with the positioning of hCD157 on the extracellular



[Nam] = 0

$$k_{obs} = \frac{k_2[NR]}{[NR] + K_D}$$

[Nam] \sim K_N

$$k_{obs} = \frac{k_2[NR]}{[NR] + K_D} + \frac{k_{-2}[Nam]}{[Nam] + K_N} + \frac{k_4K_N}{[Nam] + K_N}$$

Scheme 2. A minimal kinetic scheme describing the effect of Nam on k_{obs} .

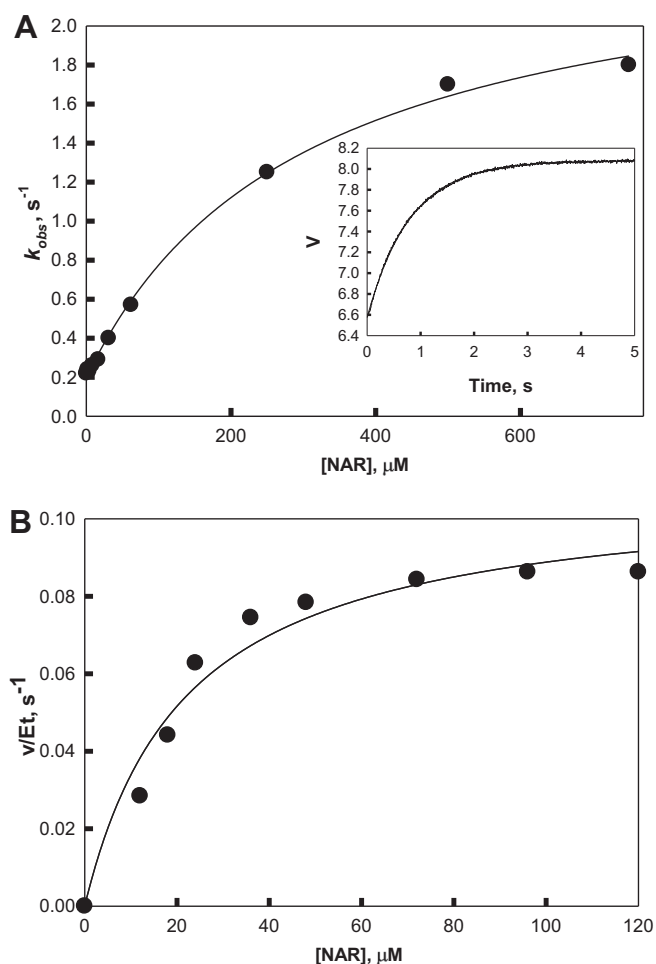


Fig. 3. (A) Pre-steady state binding of NAR to hCD157. Addition of variable concentrations of NAR to 200 nM hCD157 resulted in a first order increase in protein fluorescence ($\lambda_{\text{ex}} = 290 \text{ nm}$, $\lambda_{\text{em}} > 335 \text{ nm}$) that was dependent on [NAR]. A hyperbola was fitted to the first order rate constants. The asymptote ($2.3 \pm 0.1 \text{ s}^{-1}$, k_2) and the K_D values ($300 \pm 40 \mu\text{M}$) for initial complex formation were determined in the absence of nicotinic acid. Inset: 250 μM NAR was added to 100 nM hCD157 and the increase in protein fluorescence was monitored on the stopped-flow. A single exponential was fitted to the data. The value of k_{obs} was $1.25 \pm 0.01 \text{ s}^{-1}$ and the increase in amplitude was $1.5 \pm 0.01 \text{ V}$. (B) Initial rate analyses of NAR hydrolysis. The rate of hydrolysis of NAR in Standard Buffer was followed at 280 nm on a conventional UV–VIS spectrophotometer. Initial rates were divided by the enzyme concentration to derive v/E_t (s^{-1}). The fitted hyperbola determined a K_M value of $22 \pm 5 \mu\text{M}$ and a k_{cat} value (v/E_t) of $0.11 \pm 0.01 \text{ s}^{-1}$.

face, as phosphorylated nucleotides are usually concentrated inside the cell. The low K_M and k_{cat} values indicate that cell-surface hCD157 can act as a sensitive cell surface receptor for NR. Protein conformational changes were observed upon initial binding and were slowly reversed upon hydrolysis of $E * R$ to regenerate free E.

Hydrolysis or binding (Table 1) of NAD^+ to near full-length hCD157 protein was undetectable. In order to better understand the protein biochemistry and selectivity of NAD^+ in the context of their structures, the active sites of hCD38 and hCD157 were compared using two different methods. First we compared active sites (Fig. 4) from the published crystal structures of BST-1/CD157 (PDB code 1ISJ) and hCD38 (PDB code 3D7J) bound with NMN [29,33]. In both proteins the 3-carboxamido-pyridinium ring of NMN π -stacks with W140 in hCD157 and W189 in hCD38. The 3-carboxamido-group forms hydrogen bonds with aspartate in both active sites, D107 in hCD157 and D155 in hCD38. A potentially catalytic glutamate residue, E178 in hCD157 and E226 in hCD38, appears to be well positioned for nucleophilic attack on

the ribose moiety of NMN. hCD38 can complete the chemical displacement step, but hCD157 is unable to complete this reaction. Therefore, the sequence similarities between hCD157 and hCD38 in the active sites are necessary but not sufficient to explain catalysis, with NMN and NAD^+ as substrates. We focused our analysis on identifying changes in the active sites that may translate to differences in substrate preference. For example, S98 of hCD157 prevents the formation of a second hydrogen bond with the 3-carboxamido group of NMN, which is formed with E146 in hCD38. The large hydrophobic (F108) residue of hCD157 occludes much of the active site and is uncharged, as compared to the corresponding acidic residue (D156) in hCD38. An asparagine residue (N79) of hCD157 is a much smaller and less flexible amino acid than the corresponding arginine residue (R127) in hCD38 and is unable to form a hydrogen bond with the phosphate group of NMN. Lastly, a phenylalanine residue (F173) of hCD157 may deter productive binding of the NMN phosphate group by steric occlusion and the loss of a potential hydrogen bond. This residue is a threonine (T221) in hCD38, which hydrogen bonds to the phosphate group of NMN.

We also hypothesized that differences between the volumes and surface areas of the hCD157 and hCD38 active sites could explain the biochemical differences that were observed experimentally. Calculations of these parameters were undertaken in the context of the hCD157 and hCD38 NMN-complexes. However, because the published structure of BST-1/CD157 contains only 250 amino acids [33] and these calculations are sensitive to minor differences in the crystal structures, we experimentally determined the crystal structure of the hCD38 catalytic mutant E226Q in a complex with NMN (Supplemental Fig. 4). As expected, our crystal structure (PDB code 4OGW) showed that the active site of hCD38 is a pocket formed by both the C- and N-terminal sub-domains of the protein. The proposed catalytic glutamate E226(Q) is enclosed deep within its core. Importantly, our hCD38 E226Q structure differs from the published structure (PDB code 3DZJ) in that the side-chain orientation of L129 differs and the side-chain position of R127 is unresolved in our structure. A number of other minor differences outside the catalytic site exist but are assumed to have an insignificant impact on our calculations. The structure of hCD38 E226Q bound with NMN and the structure of the BST-1/CD157 NMN-complex were used to calculate the volume and surface area of the active sites (Supplemental Methods). The volumes of hCD157 and hCD38 active sites were calculated to be 5822 and 5870 \AA^3 while the surface areas were determined to be 3341 and 3566 \AA^2 , respectively. Both the volume and surface area calculations verified that the active site of hCD157 is smaller than that of hCD38. Dinucleotides (NAD^+) would have more difficulty binding the active site of hCD157.

Various biological functions have been ascribed to CD157 in the literature [20]. Roles in B-cell maturation, leukocyte homing, B-cell activation, rheumatoid arthritis, cellular migration, integrin-signaling, antibody-stimulated tyrosine-phosphorylation, ovarian tumor metastases, cellular responses to caloric restriction and mesenchymal stem cell proliferation have been reported [20,34–38]. Because we have identified NR as the preferred substrate of hCD157 it will be of interest to determine if any of these biological responses are affected by exposure to NR.

By extensively characterizing the hydrolytic reactions with nucleos(t)ide substrates, fNR was identified as a mechanism-based inhibitor of hCD157. The compound is a poor substrate (k_2 value of $0.04 \text{ vs } 360 \text{ s}^{-1}$) that forms a stable intermediate ($E * fR$), that cannot be easily hydrolyzed to form free enzyme (k_4 value not measurable). The natural substrate NAR [39–41] did not as bind well to the enzyme (K_D value of $300 \text{ vs } 22 \mu\text{M}$ for NR), and the rate of the induced conformational change was not as robust as that observed with NR (k_2 value of $2.3 \text{ vs } 360 \text{ s}^{-1}$). Both NR and

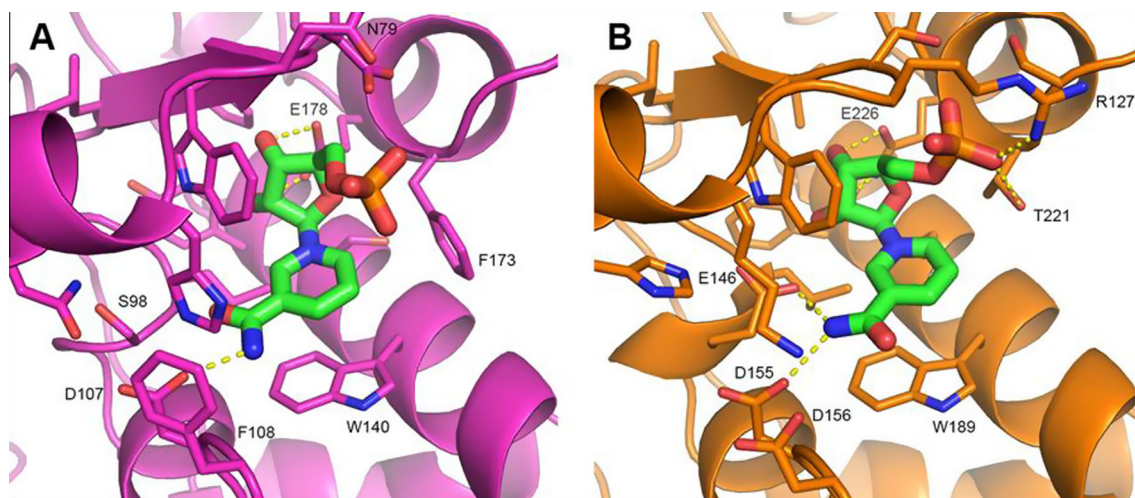


Fig. 4. Crystal structures of the active sites of BST-1/CD157 (Panel A) and hCD38 (Panel B) bound with NMN. Panel A shows the BST-1/CD157 active site (PDB code 1ISJ) bound with NMN with relevant hydrogen bonds (dashed yellow lines) displayed and critical residues labeled. Panel B displays the active site of hCD38 (PDB code 3DZJ) with relevant hydrogen bonds illustrated (dashed yellow lines) and key residues labeled. The hCD157 catalytic site contains a single acidic residue (D107) that forms a hydrogen bond with the 3-carboxamido group of NMN. The S98 residue prevents the formation of a second hydrogen bond with NMN that is observed in hCD38 (E146). F108 occludes much of the hCD157 active site, and is unchanged compared with the corresponding residue in hCD38 (D156). Additionally, the smaller and less flexible N79 (R127 in hCD38) is unable to form a hydrogen bond with the phosphate group of NMN. Lastly, unlike the hydrogen bonding pattern observed in hCD38 (T221), F173 in hCD157 prevents hydrogen bond formation with the phosphate group of NMN. (For interpretation of the references to colour in this figure legend, the reader is referred to the web version of this article.)

NAR form a catalytic intermediate ($E * R$) that was hydrolyzed by hCD157 at 0.1 s^{-1} . The differences in the rate of chemical attack (k_2) between NR, NAR and fNR support the observation that NR is a preferred substrate of hCD157. hCD157 like purine nucleoside phosphorylase [32] and uridine hydrolase [42] prefers nucleoside substrates (Table 1).

With a low measured k_{cat} value of 0.1 s^{-1} , the hCD157 catalytic intermediate ($E * R$, ribosylated enzyme) has an average half-life of approximately 7 s. The ribose-5-phosphate intermediate formed during the CD38-catalyzed hydrolysis of NMN [15] has an average half-life of milliseconds. Given the stability of the $E * R$ intermediate in aqueous solution, it is likely that the $E * R$ intermediate is covalent and not an enzyme-stabilized oxocarbenium ion. The relatively long-lived high energy $E * R$ intermediate can react with nucleophiles other than water. Because molar concentrations of methanol enhanced the turnover of NR (Supplemental Fig. 3A and B), it is of interest to identify heterocycles that can enhance the turnover of NR either through base-assisted catalysis or base-exchange reactions [16].

Inhibitors of hCD157 may prove to be useful tools to investigate the pharmacology of NR, NR-dependent signaling, and NAD^+ metabolism [6–11]. Now that NR has been identified as the preferred natural substrate of hCD157 it may be useful to test substrate analogs (NR and analogs thereof) or inhibitors of hydrolytic function for potential therapeutic efficacy in preclinical disease models. The key to success in any preclinical model will be determining the causal role of the NAD^+ deficiency in determining the disease physiology.

Acknowledgments

The authors would like to thank Curt Haffner and David Becherer for their support in characterizing CD38 inhibitors. Mark Bickett for initial preparations of NR; Yingnian Shen for cloning hCD157 into GSK Bacmam expression vectors; Scott Sigethy for preparing Bacmam virus stocks; George Barrett for large scale cell culture; Mary B. Moyer for LC/MS peptide sequencing of fNR-modified hCD157; Ginger Tomberlin for HPLC analyses; Timothy Spitzer

for NMR analyses; Richard Caldwell and Bruce Szczepankiewicz (GSK-Sirtris) for chemical synthesis of NAR.

Appendix A. Supplementary data

Supplementary data associated with this article can be found, in the online version, at <http://dx.doi.org/10.1016/j.abb.2014.09.008>.

References

- [1] A.A. Sauve, C. Wolberger, V.L. Schramm, J.D. Boeke, *Ann. Rev. Biochem.* 75 (2006) 435–465.
- [2] C.T. Jurgensen, T.P. Begley, S.E. Ealick, *Ann. Rev. Biochem.* 78 (2009) 569–603.
- [3] P. Belenky, K.L. Bogan, C. Brenner, *Trends Biochem. Sci.* 32 (2007) 12–19.
- [4] P. Belenky, K.C. Christensen, F. Gazzaniga, A.A. Pletnev, C. Brenner, *J. Biol. Chem.* 284 (2009) 158–164.
- [5] M. Zillmann, M.A. Gorovsky, E.M. Phizicky, *Mol. Cell. Biol.* 11 (1991) 5410–5416.
- [6] K.L. Eckel-Mahan, V.R. Patel, S. de Mateo, R. Orozco-Solis, N.J. Ceglia, S. Sahar, S.A. Dilag-Penilla, K.A. Dyar, P. Baldi, P. Sassone-Corsi, *Cell* 155 (2013) 1464–1478.
- [7] C. Escande, V. Nin, N.L. Price, V. Capellini, A.P. Gomes, M.T. Barboza, L. O'Neill, T.A. White, D.A. Sinclair, E.N. Chini, *Diabetes* 62 (2013) 1084–1093.
- [8] L. Mouchiroud, R.H. Houtkooper, N. Moullan, E. Katsyuba, D. Ryu, C. Cantó, A. Mottis, Y.-S. Jo, M. Viswanathan, K. Schoonjans, L. Guarente, J. Auwerx, *Cell* 154 (2013) 430–441.
- [9] C. Cantó, R.H. Houtkooper, E. Pirinen, D.Y. Yoon, M.H. Oosterveer, Y. Cen, P.J. Fernandez-Marcos, H. Yamamoto, P.A. Andreux, P. Cettour-Rose, K. Gademann, C. Rinsch, K. Schoonjans, A.A. Sauve, J. Auwerx, *Cell Metab.* 15 (2012) 838–847.
- [10] A.P. Gomes, N.L. Price, A.J.Y. Ling, J.J. Moslehi, M.K. Montgomery, L. Rajman, J.P. White, J.S. Teodoro, C.D. Wrann, B.P. Hubbard, E.M. Mercken, C. Palmeira, R. de Cabo, A.P. Rolo, N. Turner, E.L. Bell, D.A. Sinclair, *Cell* 155 (2013) 1624–1638.
- [11] J. Yoshino, K.F. Mills, M.J. Yoon, S. Imai, *Cell Metab.* 14 (2011) 528–536.
- [12] J. Goldberger, C.H. Waring, D.G. Willet, *South. Med. J.* 8 (1916) 1043–1044.
- [13] D.L. Glick, M.R. Hellmich, S. Beshausen, P. Tempst, H. Bayley, F. Strumwasser, *Cell Regul.* 2 (1991) 211–218.
- [14] A.A. Sauve, H. Deng, R.H. Angeletti, V.L. Schramm, *J. Am. Chem. Soc.* 122 (2000) 7855–7860.
- [15] A.A. Sauve, C. Munshi, H.C. Lee, V.L. Schramm, *Biochemistry* 37 (1998) 13239–13249.
- [16] F. Preugschat, G.H. Tomberlin, D.J.T. Porter, *Arch. Biochem. Biophys.* 479 (2008) 114–120.
- [17] H.C. Lee, R. Aarhus, *J. Biol. Chem.* 272 (1997) 20378–20383.
- [18] T. Kaisho, J. Isikawa, K. Oritani, J. Inazawa, H. Tomizawa, O. Muraoka, T. Ochi, T. Hirano, *Proc. Natl. Acad. Sci. U.S.A.* 91 (1994) 5325–5329.
- [19] M. Itoh, K. Ishihara, H. Tomizawa, H. Tanaka, Y. Kobune, J. Ishikawa, T. Kaisho, T. Hirano, *Biochem. Biophys. Res. Commun.* 203 (1994) 1309–1317.

- [20] V. Quarona, G. Zaccarello, A. Chillemi, E. Brunetti, V.K. Singh, E. Ferrero, A. Funaro, A.L. Horenstein, F. Malavasi, *Clin. Cytometry* 84B (2013) 207–217.
- [21] S. Yamamoto-Katayama, A. Sato, M. Ariyoshi, M. Suyama, K. Ishihara, T. Hirano, H. Nakamura, K. Morikawa, H. Jingami, *Biochem. J.* 357 (2000) 385–392.
- [22] Y. Okuyama, K. Ishihara, N. Kimura, Y. Hirata, K. Sato, M. Itoh, L.B. Ok, T. Hirano, *Biochem. Biophys. Res. Commun.* 228 (1996) 838–845.
- [23] F. Schlenk, *Naturwissenschaften* 28 (1940) 46–47.
- [24] P. Biegenowski, C. Brenner, *Cell* 117 (2004) 495–502.
- [25] Y. Chi, A.A. Sauve, *Curr. Opin. Clin. Nutr. Metab. Care* 60 (2013) 741–748.
- [26] T. Kost, P.J. Condreay, D.L. Jarvis, *Nat. Biotechnol.* 23 (2005) 567–575.
- [27] Z. Otwinowski, W. Minow, *Meth. Enzymol.* 276 (1997) 307–326.
- [28] A. Vagin, A. Teplyakov, *J. Appl. Crystallogr.* 30 (1997) 1022–1025.
- [29] Q. Liu, I.A. Kriksunov, R. Graeff, C. Munshi, H.C. Lee, Q. Hao, *Structure* 13 (2005) 1331–1339.
- [30] G.N. Murshudov, A. Vagin, E.J. Dodson, *Acta Crystallogr. D Biol. Crystallogr.* 53 (1997) 240–255.
- [31] P. Emsley, K. Cowtan, *Acta Crystallogr. D Biol. Crystallogr.* 60 (2004) 2126–2132.
- [32] B. Wielgus-Kutrowska, E. Kulikowska, J. Wierchowski, A. Bzowska, D. Sugar, *Eur. J. Biochem.* 243 (1997) 408–414.
- [33] S. Yamamoto-Katayama, M. Ariyoshi, K. Ishikara, T. Hirano, H. Jingami, K. Morikawa, *J. Mol. Biol.* 316 (2002) 711–723.
- [34] E. Ortolan, R. Arisio, S. Morone, P. Bovino, L.N. Buono, G. Nacci, R. Parrotta, D. Katsaros, I. Rapa, G. Migliaretti, E. Ferrero, M. Volante, A. Funaro, *J. Natl. Cancer Inst.* 102 (2010) 1160–1177.
- [35] F. Liang, C.F. Chang, *FEBS Lett.* 506 (2001) 207–210.
- [36] N.L. Buono, R. Parrotta, S. Morone, P. Bovino, G. Nacci, E. Ortolan, A.L. Horenstein, A. Inzhutova, E. Ferrero, A. Funaro, *J. Biol. Chem.* 286 (2011) 18681–18691.
- [37] O.H. Yilmaz, P. Katajisto, D.W. Lamming, Y. Guelekin, K.E. Bauer-Rowe, S. Senupta, K. Birsoy, A. Dursun, V.O. Yilmaz, M. Selig, G.P. Nielsen, M. Minokendson, L.R. Zukerberg, A.K. Bhan, V. Deshpande, D. Sabatini, *Nature* 486 (2012) 490–495.
- [38] E. Aomatsu, N. Takahashi, S. Sawada, N. Okubo, T. Hasegawa, M. Taira, H. Miura, A. Ishisaki, N. Chosa, *Sci. Rep.* 4 (2014) 1–9.
- [39] W. Tempel, W.M. Rabeh, K.L. Bogan, P. Belenky, M. Wojcik, H.F. Seidle, L. Nedyalkova, T. Yang, A.A. Sauve, H.-W. Park, C. Brenner, *PLoS Biol.* 5 (2007) 2220–2230.
- [40] K.L. Bogan, C. Evans, P. Belenky, P. Song, C.F. Burant, R. Kennedy, C. Brenner, *J. Biol. Chem.* 284 (2009) 34861–34869.
- [41] C. Evans, K.L. Bogan, P. Song, C.F. Burant, R. Kennedy, C. Brenner, *BMC Chem. Biol.* 10 (2010) 2–10.
- [42] P. Belenky, F.G. Racette, K.L. Bogan, J.M. McClure, J.S. Smith, C. Brenner, *Cell* 129 (2007) 473–484.